Earth and Planetary Science Letters 489 (2018) 111–122

Contents lists available at ScienceDirect

Earth and Planetary Science Letters

www.elsevier.com/locate/epsl

Addressing the contribution of climate and vegetation cover on hillslope denudation, Chilean Coastal Cordillera (26°–38°S)

M. Schaller [a,*], T.A. Ehlers [a], K.A.H. Lang [a,b], M. Schmid [a], J.P. Fuentes-Espoz [c]

[a] University of Tuebingen, Department of Geosciences, Wilhelmstrasse 56, 72074 Tuebingen, Germany
[b] Stockholm University, Department of Geological Sciences, Svante Arrhenius väg 8, 106 91 Stockholm, Sweden
[c] University of Chile, Department of Silviculture and Nature Conservation, Av. Santa Rosa 11315, La Pintana, Santiago RM, Chile

ARTICLE INFO

Article history:
Received 30 October 2017
Received in revised form 19 February 2018
Accepted 20 February 2018
Available online 8 March 2018
Editor: A. Yin

Keywords:
denudation
hillslope
climate
biota
cosmogenic nuclide
Chile

ABSTRACT

The Earth surface is modulated by interactions among tectonics, climate, and biota. The influence of each of these factors on hillslope denudation rates is difficult to disentangle. The Chilean Coastal Cordillera offers a strong climate and vegetation gradient from arid and unvegetated in the North to humid and vegetated in the South. A similar (convergent) plate tectonic boundary lies to the West of the Coastal Cordillera. We present eight depth profiles analyzed for *in situ*-produced cosmogenic ^{10}Be in four study areas. These profiles reveal denudation rates of soil-mantled hillslopes and the depth of mobile layers. Depth profiles were investigated from both S- and N-facing mid-slope positions. Results indicate the depth of the mobile layers in the four study areas increase from N to S in latitude. When mixing is present in the mobile layers they are completely mixed. In the S- and N-facing hillslopes of each study area, mid-slope positions do not show a systematic change in depth of the mobile layers nor in denudation rates based on cosmogenic depth profiles. From N to S in latitude, modelled denudation rates of hillslopes increase from ~0.46 to ~5.65 cm/kyr and then decrease to ~3.22 cm/kyr in the southernmost, highest vegetation cover, study area. Calculated turnover times of soils decrease from ~30 to ~11 kyr and then increase to ~22 kyr. In this work, the increasing denudation rates are attributed to increasing mean annual precipitation from N to S. However, despite the ongoing increase in precipitation from N to S, the denudation rate in the southernmost location does not continue to increase due to the protective nature of increasing vegetation cover. This indicates a vegetation induced non-linear relationship with denudation rates.

1. Introduction

The Earth surface, where atmosphere, lithosphere, water, and life interact, is governed by tectonic and climatic processes. However, climate conditions affect biota (fauna and flora), which in turn influences physical erosion (e.g., soil mixing by bioturbation, rain splash, tree throw, soil creep) and chemical weathering processes (e.g., mineral dissolution by microbial activity and/or acidity). These complex and often non-linear interactions as well as their effect on Earth surface processes are difficult to study and quantify (e.g., Corenblit et al., 2011). One avenue to study and quantify Earth surface processes is the application of cosmogenic nuclides.

Measurements of cosmogenic nuclide concentrations enable quantitative determination of rates of Earth surface processes over a wide variety of spatial scales, from catchment-wide denudation rates from measurements of river sediments (e.g., Brown et al., 1995; Granger et al., 1996) to soil production rates from measurements of saprolite (e.g., Heimsath et al., 1997). Soil production rates (i.e. the rate of conversion of saprolite to soil) can be calculated from the cosmogenic nuclide concentration of saprolite located at the interface between the mobile and immobile layers of a depth profile (Fig. 1). This calculation assumes steady-state conditions of constant soil production, soil depth, soil bulk density, and identifies the degree of mixing within the soil layer (e.g., Heimsath et al., 1997; Granger et al., 1996; Schaller et al., 2009). While visual verification of possible mixing of the mobile layer is not easy, measurements of several samples in a cosmogenic depth profile can evaluate the depth of mixing. In the case of no mixing, the cosmogenic nuclide concentration decreases exponentially with depth (Fig. 1). In the case of well-mixing, the cosmogenic nuclide concentration in the mixed soil layer is homogeneous. Furthermore, the knowledge of the denudation rate based on depth profiles and the depth of the mobile layer allow the calculation of

* Corresponding author.
E-mail address: mirjam.schaller@uni-tuebingen.de (M. Schaller).

https://doi.org/10.1016/j.epsl.2018.02.026
0012-821X/

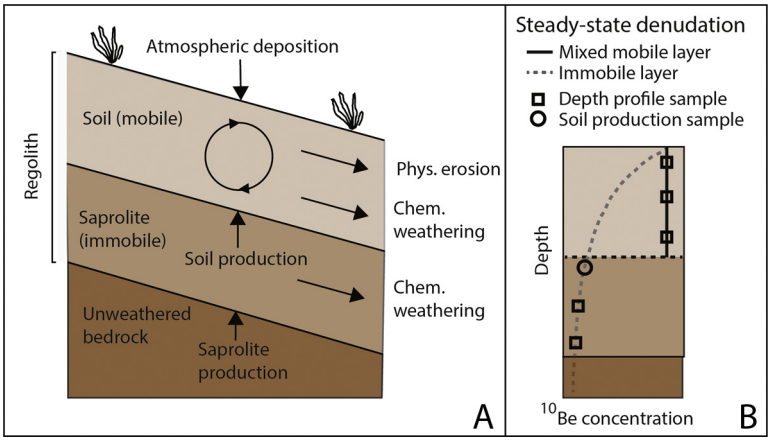

Fig. 1. Schematic view of a steady-state eroding soil-mantled hillslope. A) The unweathered bedrock is overlain by the regolith which consists of the immobile saprolite and the mobile soil, B) The *in situ*-produced ^{10}Be concentration is homogeneous in a well-mixed mobile soil whereas the concentration decreases exponential with depth in the immobile saprolite. Several samples (squares) need to be collected for depth profile analysis, whereas only one sample (point) is required for the determination of the soil production rate.

the soil turnover time (Fig. 1). The soil turnover time is the time a mineral grain resides in average in the mobile layer before it is getting eroded.

Owen et al. (2011) investigate the climatic and biotic influences on soil production rates in soil-mantled hillslopes in the Chilean Coastal Cordillera (Fig. 2) by comparing measurements from tectonically similar settings. As previous work, this study focuses on the Coastal Cordillera because of similar lithologies exposed along its approximate 3000 km length, and the similar (convergent) plate boundary to the West where subduction of the Nazca (and formerly Farallon) plate have been ongoing over hundred-million-year timescales. Thus, the western South America plate boundary provides one of the most spatially and temporally consistent plate tectonic settings possible over a large range of latitudes. Furthermore, a dramatic latitudinal gradient in precipitation rates is present along the Coastal Cordillera and produces diverse vegetation zones. Owen et al. (2011) determined soil production rates on active soil-mantled hillslopes located around our northernmost study area. Their sampling is located in three climatically different regions including: 1) hyper arid (~24°S); 2) arid (~26°S); and 3) semi-arid (~30°S). Whereas mean annual precipitation increases from <2 mm/yr to 119 mm/yr, the vegetation

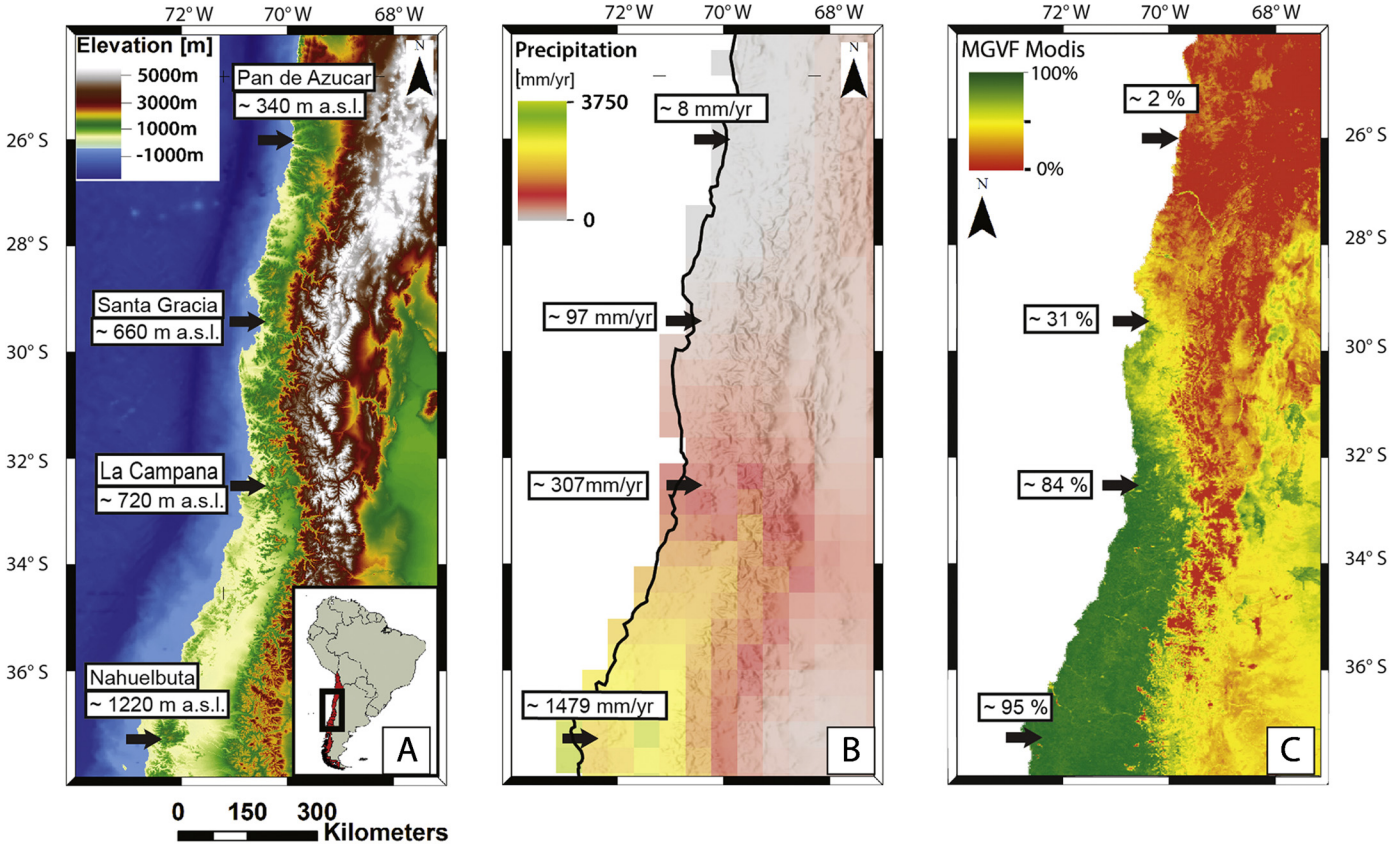

Fig. 2. Overview of the four study areas located in the Chilean Coastal Cordillera shown from 24° to 38°S: A) Digital elevation model showing from N to S the location of Pan de Azúcar, Santa Gracia, La Campana, and Nahuelbuta; B) Mean annual precipitation (Karger et al., 2017); C) Relative vegetation cover (Broxton et al., 2014). From N to S the mean annual precipitation rate and the relative vegetation cover increase from 8 to 1479 mm/yr and ~2 to ~95%, respectively.

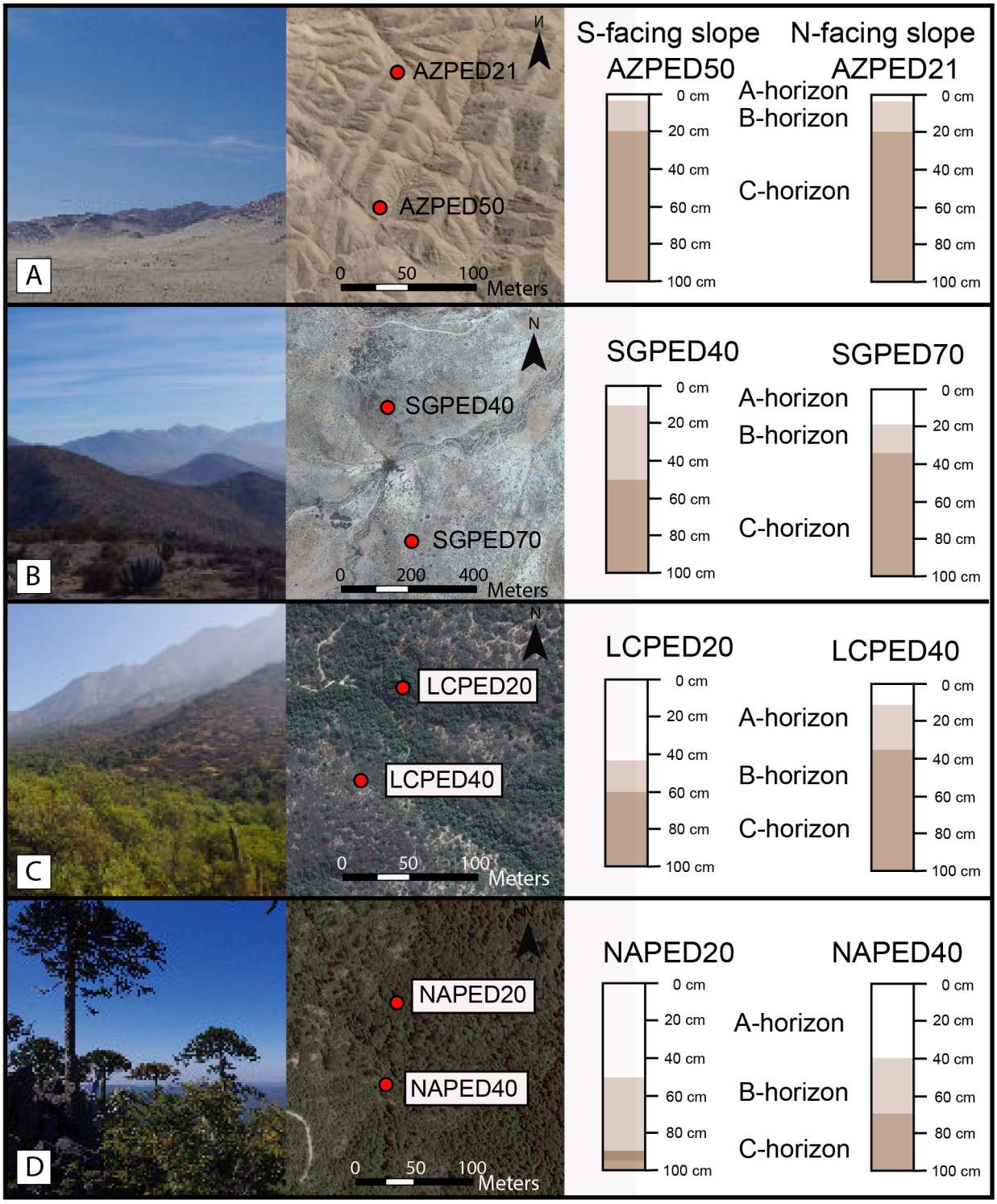

Fig. 3. Photographs of the four study areas (general view), Google Earth image of sample locations, and pedon depths in the S- and N-facing mid-slope profiles: A) Pan de Azúcar; B) Santa Gracia; C) La Campana; and D) Nahuelbuta.

cover increases from 0% to 32% of the surface area. Soil production rates were observed to increase N to S from ~0.1 cm/kyr over ~0.3 cm/kyr to ~4.0 cm/kyr (Owen et al., 2011). The processes involved in changes in denudation rates range from abiotic (e.g., salt shrink-swell, overland flow) to biotic (bioturbation, bio facilitated chemical weathering) indicating that hillslope bedrock denudation is sensitive to increasing precipitation and biotic input.

In this study, we utilize the large climate and vegetation gradient in the Chilean Coastal Cordillera (26 to 38°S; Figs. 2 and 3) to quantify interactions between climate and biota on denudation. We perform measurements in four field sites selected with a similar tectonic setting and granodiorite rock type, but different climates and hence biota. We measured *in situ*-produced ^{10}Be in multiple depth profiles on S- and N-facing hillslopes to study the depth of mixed layers, millennially-averaged denudation rates, and soil turnover times for different mean annual precipitation rates and temperatures as well as vegetation cover. Here we compare depth profiles from S- and N-facing hillslopes across all four

Table 1
Information about soil pedons located in four study areas.

Location	Latitude (°S)	Longitude (°W)	Sample alt. (m a.s.l.)	Aspect (°)	Slope (°)	Precipitation (mm/yr)	Temperature (°)	Vegetation cover (°)
Pan de Azucar								
AZPED50	26.11012	70.54922	333	0	40	8	20.1	2
AZPED21	26.10936	70.54907	342	180	25	8	20.1	2
Santa Gracia								
SGPED40	29.75738	71.16635	682	0	25	97	17.7	31
SGPED70	29.76120	71.16559	690	180	15	97	17.7	31
La Campana								
LCPED20	32.95588	71.06355	718	0	23	307	14.1	84
LCPED40	32.95720	71.06425	724	120	12	307	14.1	84
Nahuelbuta								
NAPED20	37.80770	73.01257	1239	60	15	1479	6.1	95
NAPED40	37.80904	73.01380	1219	180	13	1479	6.1	95

locations to test three hypotheses related to biotic and climatic controls on denudation. These hypotheses include: i) that mobile layers of soil-mantled hillslopes identified in the field are well-mixed; ii) that mixed layer thickness and denudation rates vary from S- to N-facing hillslopes (e.g., Riebe et al., 2017); and iii) that denudation rates increase, and soil turnover times decrease, with increasing mean annual precipitation from N to S in the Chilean Coastal Cordillera.

2. Study areas and characteristics of depth profiles

The four investigated study areas are situated in the Chilean Coastal Cordillera and have a latitudinal extent ranging over ~1,300 km from ~26 to ~38°S (Fig. 2). This latitudinal extent results in climate and vegetation gradients covering arid to humid conditions and sparse to temperate rainforest vegetation cover, respectively (Fig. 3; Table 1). A comparable climate gradient existed also during the Last Glacial Maximum with higher precipitations than present, but still increasing from N to S (see Supplementary Fig. S1; Mutz et al., 2017). In addition, none of the study areas are or were glaciated. Furthermore, these study areas were selected because they are national parks or nature preserves and have minimal anthropogenic influence.

The influence of these different conditions on active soil-mantled hillslopes is investigated here with soil pedons excavated from mid-slope positions. The two pedons for each study area are located in a S- and a N-facing slope position with as much as possible similar hillslope angles (Table 1). Unfortunately, as hillslope angles are variable this possible influence will be addressed. The S- and N- facing slopes were collected on opposite sides of a valley or ridge and are typically located within ~200 m of each other and on hillslopes with ~10 to 100 m of relief (see also Supplementary Table S1). For comparison of data, the four selected study areas are located in areas with granitic to granodioritic lithologies and similar tectonic conditions (subduction zone). The modelled surface uplift rates of the Chilean coast between Pan de Azúcar (~26°S) and La Campana (~33°S) range between 10 to 20 cm/kyr (Melnick, 2016). Between La Campana and Nahuelbuta (~38°S), the uplift rates are very variable and can be as high as 400 cm/kyr (e.g., Jara-Muñoz et al., 2015). Over longer (geologic) timescales, thermochronometer cooling age data from the Coastal Cordillera are limited and provide an incomplete picture of the tectonic history of this range. What is known from available apatite (U–Th)/He thermochronometer samples collected in northern Chile (Juez-Larré et al., 2010) is that the most recent phase of rock cooling (and tectonic activity by inference) was between 40–50 Ma suggesting minor tectonic activity since then as deformation migrated to the eastern flank of the Andean Plateau (Barnes and Ehlers, 2009). Differences in hillslope, lithology, and tectonics from one study area to the other are kept as small as possible, and one of the best environments one could hope to sample over the large (12°) latitudinal range is considered in this study. However, we acknowledge that additional work is needed (e.g. via thermochronology) to improve documentation of the tectonic history. Changes in climate and vegetation are therefore considered to be the dominant factors that influence denudation rate, mobile layer thickness, and weathering rate in this area.

Observations from the S- and N-facing mid-slope pedons of each study area are discussed below. The regolith consists of both an immobile layer of weathered saprolite and a mobile layer on top (Fig. 1). This mobile surface layer is considered hereafter as soil (e.g., Granger and Riebe, 2014) and generally consists of an A- and a B-horizon (Fig. 3). The depth to the unweathered bedrock is not observed in outcrops in any of the study areas, but could be as deep as 3000 cm (e.g., Vázquez et al., 2016). Furthermore, field observations of road cuts and quarries outside of study areas indicate weathered bedrock to 10's of meters depth (or more). Soil bulk densities used in this study are from Bernhard et al. (in review).

2.1. Pan de Azúcar study area

The Pan de Azúcar study area (Fig. 3A), is located at ~340 m above sea level (a.s.l.), has a mean annual precipitation (MAP) of 8 mm/yr, and a mean annual temperature (MAT) of 20.1 °C (Karger et al., 2017). The sparse flora in this area (vegetation cover of ~2%; Broxton et al., 2014) is dominated by *Nolana flaccida* (Solanaceae), *Loasa chilensis* (Loasaceae), and *Heliotropium linearifolium* (Boraginaceae). The plant species *N. Flaccida* is able to excrete salts on its leaves, allowing collection of atmospheric moisture (Thompson et al., 2003). No burrowing mammals are described for Pan de Azúcar. The S-facing mid-slope pedon is located on a topographic slope of 40°. Field observations of the saprolite to soil transition suggest a mobile layer depth of 20 cm. The average bulk density of the mobile layer is 1.47 g/cm^3. The mobile layer in the N-facing mid-slope pedon is 20 cm thick and has an average bulk density of 1.31 g/cm^3. The topographic slope of this position is 25°.

2.2. Santa Gracia study area

The S- and N-facing pedons in Santa Gracia (Fig. 3B) are situated at 632 and 690 m a.s.l., respectively. A MAP of 97 mm/yr and a MAT of 17.7 °C (Karger et al., 2017) in this area result in a vegetation cover of ~31% (Broxton et al., 2014). According to Luebert and Pliscoff (2006), natural vegetation corresponds to mediterranean desertic shrubs dominated by *Adesmia argentea* (Fabaceae) and *Bulnesia chilensis* (Zygophyllaceae). Potential burrowing mammals in this area are *Spalacopus cyanus* (Octodontidae) and *Octodon degus*

(Octodontidae). Whereas the former burrows tunnels in 10 to 15 cm below surface (e.g., Begall and Gallardo, 2000), the latter burrows from 15 to 60 cm depth (e.g. Ebensperger et al., 2011). The S- and N-facing mid-slope pedons have topographic slopes of 25° and 15°, respectively. Whereas the mobile layer of the S-facing pedon is 50 cm thick and has an average bulk density of 1.48 g/cm^3, the mobile layer of the N-facing pedon is 35 cm thick and has an average bulk density of 1.58 g/cm^3.

2.3. La Campana study area

In the La Campana study area (Fig. 3C), the S- and N-facing mid-slope pedons are located at an altitude of ~720 m a.s.l. The MAP and MAT are 307 mm/yr and 14.1 °C, respectively (Karger et al., 2017). The flora, with a vegetation cover of ~84% (Broxton et al., 2014), changes as a function of slope aspect. In S-facing slopes, vegetation is dominated by sclerophylous trees and shrubs of *Quillaja saponaria* (Rosaceae) and *Lithraea caustica* (Anacardiaceae). In the xeric N-facing slopes, dominant species are plants of *Puya berteroniana* (Bromeliaceae) and *Trichocereus chiloensis* (Cactaceae), conforming to a more open vegetation ecosystem than in the S-facing slopes (Rundel and Weisser, 1975; Hauck et al., 2016). The palm *Jubaea chilensis* (Arecaceae) can be found in both plant community types, but occupying a small proportion of the surface. As in Santa Gracia potential burrowing animals in this area are *Spalacopus cyanus* (Octodontidae) and *Octodon degus* (Octodontidae). The mobile layer in the S-facing mid-slope pedon (23° slope gradient) has a thickness of 65 cm and an average bulk density of 1.11 g/cm^3. The mobile layer in the N-facing mid-slope pedon (12° slope gradient) has a thickness of 35 cm and an average bulk density of 1.47 g/cm^3.

2.4. Nahuelbuta study area

In Nahuelbuta (Fig. 3D), the southern-most study area of the four, the mid-slope pedons are at an altitude of 1239 m and 1200 m a.s.l. The MAP is 1479 mm/yr and the MAT is 6.1 °C, respectively (Karger et al., 2017). The flora, is dominated by *Araucaria araucana* (Araucariaceae), with some individuals over 1000 years old, and *Nothofagus dombeyi* (Fagaceae) constituting a mixed forest (Zamorano-Elgueta et al., 2012) with a vegetation cover that reaches ~95% (Broxton et al., 2014). Burrowing animals that can be found in Nahuelbuta are *Chelemys megalonyx* (Sigmodontinae), *Geoxus valdivianus* (Cricetidae), and *Aconaemys fuscus* (Octodontidae). *Aconaemys fuscus* (Octodontidae) burrows in 20 to 25 cm depth (Ebensperger and Bozinovic, 2000). The burrowing depths of *Chelemys megalonyx* (*Sigmodontinae*) and *Geoxus valdivianus* (*Cricetidae*) are not reported (e.g., Teta et al., 2015a and 2015b). The mobile layer of the S-facing mid-slope pedon at a position with 15° topographic slope is 70 cm thick and has an average bulk density of 0.84 g/cm^3. The mobile layer of the N-facing mid-slope pedon (13° slope) is 70 cm thick and has an average bulk density of 0.90 g/cm^3.

3. Methods

3.1. Sample collection, preparation, and analysis

At each study area two pedons were excavated from soil-mantled eroding hillslopes: One on a S-facing hillslope and another on a N-facing hillslope, both in a mid-slope position. The pedons were excavated by pick axe and jackhammer to reach depths of close to 200 cm. Generally, the grain size <2 mm was sampled. In cases of a compact material, saprolite clasts were collected. The dried sand fraction is sieved into different grain sizes (0.25–0.5, 0.5–1, and 1.0–2.0 mm). The fraction 1.0–2.0 mm was further crushed to 0.25–1.0 mm. Saprolite material was crushed and sieved into 0.25–1.0 mm fraction. In the case of the S-facing pedons, grain size fractions from ~20 cm depth were treated separately to analyze the nuclide concentration in different grain sizes in order to study potential different behavior of different grain sizes during soil mixing. Quartz material was separated from other minerals by magnetic separation. Acid leaching (hydrofluoric and nitric acid) was used for further cleaning as well as etching for meteoric ^{10}Be. After addition of ~0.3 mg ^{9}Be (GFZ ^{9}Be carrier; ^{10}Be/^{9}Be $< 1 \times 10^{-15}$) the samples were dissolved with hydrofluoric acid. ^{10}Be was separated from other elements with column chromatography and precipitation. BeO is mixed with Nb-powder for measurement of ^{10}Be/^{9}Be ratios at the accelerator mass spectrometer (AMS) facility at the University of Cologne. The ^{10}Be concentrations are corrected for machine and chemistry blanks (3.4×10^4 atoms).

3.2. Model simulation of ^{10}Be concentrations with depth

In a depositional setting, depth profiles of ^{10}Be concentrations can be used to determine age, denudation rate, and nuclide inheritance in the sediment (e.g., Hidy et al., 2010). However, in an eroding soil-mantled landscape which is in steady-state, the assumption is made that the age of the surface is infinitive and a nuclide inheritance non-existing (e.g., Cui et al., 2016). Fresh bedrock material on its way to the Earth surface is transformed into saprolite and soil which is mixed and eroded at the soil surface (Fig. 1). During this transport, the rock, saprolite, and soil material are bombarded by secondary cosmic rays due to which *in situ*-produced cosmogenic ^{10}Be is produced in quartz. The nuclide concentrations (atoms/g$_{(qyz)}$) with depth (cm) are modelled for different denudation rates (cm/kyr) and mixing depths (cm) under given densities (g/cm^3). A chi-square analysis of measured and modelled nuclide concentrations with MATLAB® provides the best solution for denudation rate and mixing depth. Based on this denudation rate and mixing depth the turnover time (kyr) can be calculated (Riebe and Granger, 2013).

Assumptions made in this study are that denudation rates, soil mixing depths, and densities in a given depth are constant over time. However, soil and saprolite densities vary with depth (e.g., Table 2), and typically increase with depth. For simplification, a four-box model is used in our calculations to account for different densities in the pedon:

- Box 1 contains the soil layer observed in the field and the calculated average bulk density based on densities measured in the soil (Bernhard et al., in review).
- Box 2 includes the saprolite layer observed in the field and the average bulk density based on densities measured in the saprolite (Bernhard et al., in review) or an assumed bulk density of 1.6 g/cm^3.
- Box 3 is based on a saprolite layer with a bulk density of 1.6 g/cm^3 to an assumed depth of 3000 cm (e.g., Vázquez et al., 2016).
- Box 4 is assumed to be bedrock with a density of 2.6 g/cm^3 from 3000 to 5000 cm.

For each depth, a cumulative bulk density of the material above the sample is calculated. Decay of ^{10}Be (Chmeleff et al., 2010; Korschinek et al., 2010) during transport to the surface is accounted for. The ^{10}Be concentration in the mixed layer is equal to concentration at the surface (Granger et al., 1996). Sea level-high latitude (SLHL) production rates are 3.92, 0.012, and 0.039 atoms/(g$_{(qtz)}$ yr) for nucleonic, stopped muonic, and fast muonic ^{10}Be production, respectively (Borchers et al., 2016; Braucher et al., 2011). The scaling factors from SLHL production rate to sample

Table 2
Sample informations and nuclide concentrations of depth profiles.

Sample	IGSN	Sample depth (cm)	Density (g/cm^3)	Mass qtz (g)	Mass ^{9}Be (10^{19} atoms)	^{10}Be concentration (10^5 atoms/$g_{(qtz)}$)
Pan de Azucar, S-facing mid-slope						
AZPED50_0-5	*GFTE1000E*	*2.5 ± 2.5*	*1.35*	8.31	*2.186*	*5.57 ± 0.20*
AZPED50_15-20(1000-2000)	*GFTE1001B*	*17.5 ± 10.0*	*1.59*	6.35	*2.182*	*4.78 ± 0.20*
AZPED50_20-25	GFTE10006	22.5 ± 10.0		34.67	*2.188*	3.86 ± 0.12
AZPED50_60-65	GFTE1000F	62.5 ± 10.0		31.05	2.181	3.33 ± 0.11
AZPED50_140-150	GFTE1000G	145.0 ± 20.0		64.43	2.184	1.52 ± 0.05
Pan de Azucar, N-facing mid-slope						
AZPED21_0-5	*GFTE1000H*	*2.5 ± 2.5*	*1.21*	14.59	*2.207*	*5.99 ± 0.21*
AZPED21_10-15	*GFTE1000J*	*12.5 ± 10.0*	*1.32*	16.70	*2.190*	*5.62 ± 0.18*
AZPED21_35-40	GFTE10007	37.5 ± 10.0		38.12	2.186	4.50 ± 0.14
AZPED21_70-80	GFTE1000K	75.0 ± 20.0		40.95	2.189	3.37 ± 0.11
AZPED21_90-100	GFTE1000L	95.0 ± 20.0		42.26	2.189	2.89 ± 0.10
Santa Gracia, S-facing mid-slope						
SGPED40_0-5	*GFTE1000M*	*2.5 ± 2.5*	*1.51*	16.34	*2.057*	*2.84 ± 0.11*
SGPED40_20-25(250–500)	*GFTE1001C*	*22.5 ± 10.0*	*1.47*	6.83	*2.043*	*2.99 ± 0.14*
SGPED40_20-25(500–1000)	*GFTE1001C*	*22.5 ± 10.0*	*1.47*	1.45	*2.047*	*2.69 ± 0.29*
SGPED40_20-25(1000–2000)	*GFTE1001C*	*22.5 ± 10.0*	*1.47*	5.87	*2.180*	*2.90 ± 0.15*
SGPED40_40-45	*GFTE1001D*	*42.5 ± 10.0*	*1.43*	21.80	*2.042*	*2.79 ± 0.10*
SGPED40_60-65	GFTE10008	62.5 ± 20.0		18.17	2.037	2.02 ± 0.08
SGPED40_120-125	GFTE1000N	122.5 ± 20.0		31.74	2.029	1.16 ± 0.05
SGPED40_190-195	GFTE1000P	192.5 ± 20.0		36.19	2.039	0.67 ± 0.03
Santa Gracia, N-facing mid-slope						
SGPED70_0-5	*GFTE1000Q*	*2.5 ± 2.5*	*1.53*	27.33	*2.208*	*3.81 ± 0.13*
SGPED70_20-25	*GFTE1000R*	*22.5 ± 10.0*	*1.52*	35.83	*2.176*	*4.45 ± 0.15*
SGPED70_35-40	GFTE10009	37.5 ± 10.0	1.66	26.43	*2.192*	3.52 ± 0.12
SGPED70_75-80	GFTE1000S	77.5 ± 20.0		19.63	2.189	2.34 ± 0.09
SGPED70_190-195	GFTE1000T	192.5 ± 20.0		6.05	2.186	0.84 ± 0.09
La Campana, S-facing mid-slope						
LCPED20_0-5	*GFTE10012*	*2.5 ± 2.5*	*0.76*	26.47	*2.181*	*1.30 ± 0.05*
LCPED20_20-25(125–250)	*GFTE1001E*	*22.5 ± 10.0*	*1.19*	21.40	*2.179*	*1.31 ± 0.05*
LCPED20_20-25(250–500)	*GFTE1001E*	*22.5 ± 10.0*	*1.19*	26.50	*2.179*	*1.31 ± 0.05*
LCPED20_20-25(500–1000)	*GFTE1001E*	*22.5 ± 10.0*	*1.19*	25.82	*2.186*	*1.25 ± 0.05*
LCPED20_20-25(1000–2000)	*GFTE1001E*	*22.5 ± 10.0*	*1.19*	17.83	*2.187*	*1.12 ± 0.05*
LCPED20_40-45	*GFTE1000A*	42.5 ± 10.0	1.40	31.07	2.208	1.20 ± 0.05
LCPED20_60-65	GFTE1000V	62.5 ± 20.0	1.43	31.38	2.192	0.91 ± 0.04
LCPED20_100-105	GFTE1000W	102.5 ± 20.0	1.47	28.59	2.187	0.55 ± 0.03
LCPED20_175-180	GFTE1000X	177.5 ± 20.0		50.25	2.187	0.32 ± 0.02
La Campana, N-facing mid-slope						
LCPED40_0-5	*GFTE1000Y*	*2.5 ± 2.5*	*1.25*	30.25	*2.192*	*0.90 ± 0.04*
	GFTE1000Y	*2.5 ± 2.5*	*1.25*	30.65	*2.195*	*0.92 ± 0.04*
LCPED40_20-25	*GFTE1000Z*	*22.5 ± 10.0*	*1.45*	26.50	*2.180*	*0.84 ± 0.04*
LCPED40_40-45	GFTE1000B	42.5 ± 10.0	1.45	31.65	*2.197*	*0.89 ± 0.04*
LCPED40_80-85	GFTE10010	82.5 ± 20.0	1.69	31.63	*2.190*	0.98 ± 0.04
	GFTE10010	82.5 ± 20.0	1.69	28.10	2.193	1.03 ± 0.04
LCPED40_130-135	GFTE10011	132.5 ± 20.0	1.42	51.43	2.186	0.48 ± 0.02
Nahuelbuta, S-facing mid-slope						
NAPED20_0-5	*GFTE1000U*	*2.5 ± 2.5*	*0.68*	16.76	*2.050*	*3.18 ± 0.14*
NAPED20_20-25(125–250)	*GFTE1001F*	*22.5 ± 10.0*	*0.76*	5.17	*2.048*	*3.35 ± 0.20*
NAPED20_20-25(500–1000)	*GFTE1001F*	*22.5 ± 10.0*	*0.76*	16.78	*2.041*	*2.96 ± 0.11*
NAPED20_20-25(1000–2000)	*GFTE1001F*	*22.5 ± 10.0*	*0.76*	19.72	*2.045*	*3.33 ± 0.12*
NAPED20_65-70	*GFTE10013*	*67.5 ± 20.0*	*1.18*	24.90	*2.041*	*3.16 ± 0.11*
NAPED20_80-85	GFTE1000C	82.5 ± 20.0	1.07	25.29	2.037	1.73 ± 0.07
NAPED20_140-145	GFTE10014	142.5 ± 20.0	1.05	8.05	2.037	1.17 ± 0.08
NAPED20_200-205	GFTE10015	202.5 ± 20.0		60.42	2.035	0.54 ± 0.02
Nahuelbuta, N-facing mid-slope						
NAPED40_0-5	*GFTE10016*	*2.5 ± 2.5*	*0.79*	32.10	*2.188*	*3.43 ± 0.12*
NAPED40_20-25	*GFTE10017*	*22.5 ± 10.0*	*0.96*	30.38	2.183	3.83 ± 0.13
NAPED40_60-65	*GFTE10018*	*62.5 ± 10.0*	*1.15*	30.85	*2.187*	*5.16 ± 0.17*
	GFTE10018	*62.5 ± 10.0*	*1.15*	31.35	2.200	*5.36 ± 0.17*
NAPED40_80-85	GFTE1000D	82.5 ± 20.0	1.22	31.30	*2.186*	3.72 ± 0.13
NAPED40_180-185	GFTE10019	182.5 ± 20.0		52.11	*2.193*	2.69 ± 0.09

Samples in italics are considered to be collected from the mobile layer.

locations are based on the online tool of Marrero et al. (2016) using the scaling procedure SA based on Lifton et al. (2014). Depth scaling of the production rates is based on nucleonic, stopped muonic, and fast muonic adsorption lengths which are 157, 1500, and 4320 g/cm^2, respectively (Braucher et al., 2011). No shielding by topography (less than 1%) and snow has been taken into account, whereas shielding by vegetation of 2.3% and 7.3% have been used in La Campana and Nahuelbuta, respectively (Plug et al., 2007).

4. Results

Nuclide concentrations from different depths for eight pedons are shown (Fig. 4; Table 2). These pedons are mid-slope positions for the S-facing and N-facing locations in the four study areas. Model simulations based on denudation rate and mixing depth for the best solution of the measured nuclide concentrations are presented (Table 3).

4.1. Pan de Azúcar

The nuclide concentrations in the S-facing pedon (AZPED50) range from 5.57×10^5 atoms/$g_{(qtz)}$ at 2.5 cm depth to 1.52×10^5 atoms/$g_{(qtz)}$ at 145 cm depth. With depth, the nuclide concentrations decrease in accordance with an exponential function. No homogeneous surface layer can be detected, but also not be excluded. The grain size analysis of the sample from 15 to 20 cm depth was only successful for one grain size (1.0–2.0 mm). Not enough quartz material for analysis was available for other grain sizes. Model calculations result in a best solution for a denudation rate of 0.58 ± 0.03 cm/kyr and a mixing of the surface layer to 17.5 cm. The calculated turnover time is 30 ± 2 kyr.

The nuclide concentrations in the N-facing pedon (AZPED21) decrease exponentially with depth from 5.99×10^5 atoms/$g_{(qtz)}$ at 2.5 cm depth to 2.89×10^5 atoms/$g_{(qtz)}$ at 95 cm depth. The available nuclide concentrations do not indicate a mixed soil layer. Model simulations result in a best-fit solution for a denudation rate of 0.46 ± 0.02 cm/kyr and no mixing of the soil layer. Because no mixing of the soil layer offers the best solution, no turnover time can be calculated.

4.2. Santa Gracia

In the S-facing pedon (SGPED40) the nuclide concentrations range from 2.99×10^5 atoms/$g_{(qtz)}$ at 22.5 cm depth to 0.67×10^5 atoms/$g_{(qtz)}$ at 192.5 cm depth. The nuclide concentrations from samples from the surface to ∼50 cm depth are within one sigma error of each other indicating mixing processes in a mobile layer. The nuclide concentrations of samples below this layer decrease exponentially. Nuclide concentrations of different grain sizes at 22.5 cm depth are within error. Model simulations of the measured concentrations result in a best solution for a denudation rate of 1.63 ± 0.09 cm/kyr, a mixing of the surface layer to 45.0 cm, and a calculated turnover time of 28 ± 2 kyr.

The nuclide concentrations in the N-facing pedon (SGPED70) are generally higher than in the S-facing pedon for comparable depths. The concentrations range from 4.45×10^5 atoms/$g_{(qtz)}$ at 22.5 cm depth to 0.84×10^5 atoms/$g_{(qtz)}$ at 192.5 cm depth. The nuclide concentration at 22.5 cm depth is higher than the concentration from samples above and below. Despite this heterogeneity of concentrations in the surface layer, a possible mixing depth of 40 to 70 cm depth was calculated. Model simulations result in a best-fit to the data for a denudation rate of 1.05 ± 0.05 cm/kyr, a mixing of the surface layer to 25.0 cm, and a turnover time of 24 ± 1 kyr.

4.3. La Campana

The S-facing pedon in La Campana (LCPED20) contains nuclide concentrations of 1.32×10^5 atoms/$g_{(qtz)}$ at 22.5 cm depth to 0.32×10^5 atoms/$g_{(qtz)}$ at 177.5 cm depth. The nuclide concentrations of different grain sizes at 22.5 cm depth are within error except for the grain size fraction of 1.0 to 2.0 cm. The possibility of a mixed surface layer of 50 to 60 cm depth is suggested by the nuclide concentrations. The best solution for the model simulations is reached with a denudation rate of 4.25 ± 0.23 cm/kyr, a mixing of the surface layer to 47.5 cm, and a calculated turnover time of 11 ± 1 kyr.

In the N-facing pedon (LCPED40), a range of nuclide concentrations from 10.3×10^5 atoms/$g_{(qtz)}$ at 82.5 cm depth to 0.48×10^5 atoms/$g_{(qtz)}$ at 132.5 cm depth. The measured nuclide concentrations indicate the possibility of a mixed surface layer up to 90 to 130 cm depth. The best solution for model simulations is achieved with a denudation rate of 5.65 ± 0.30 cm/kyr, a mixing of the surface layer to 85.0 cm, and a turnover time of 15 ± 1 kyr.

4.4. Nahuelbuta

The S-facing pedon in Nahuelbuta (NAPED20) has a range of nuclide concentrations from 3.35×10^5 atoms/$g_{(qtz)}$ at 22.5 cm depth to 0.54×10^5 atoms/$g_{(qtz)}$ at 202.5 cm depth. The nuclide concentrations of different grain sizes at 22.5 cm depth are almost within 1 sigma error. The measured nuclide concentrations indicate the possibility of a mixed surface layer to 70 to 80 cm depth. Model simulations result in a best solution for a denudation rate of 3.22 ± 0.13 cm/kyr, a mixing of the surface layer to 70 cm, and a calculated turnover time of 22 ± 1 kyr.

For the N-facing pedon (NAPED40), the highest nuclide concentration of 5.36×10^5 atoms/$g_{(qtz)}$ at 62.5 cm is measured. This concentration is distinctly higher than the concentrations measured in samples from above and below. At a depth of 182.5 cm, the nuclide concentration is 2.69×10^5 atoms/$g_{(qtz)}$. A best solution for the model simulations of this depth profile was not possible.

5. Discussion

5.1. Synthesis of cosmogenic nuclide concentrations and model simulations

When soils meet assumed steady-state conditions for the soil production and denudation rates, then cosmogenic nuclide concentrations are expected to be homogeneous with depth in the mobile soil layer and decrease exponentially below this layer (Granger et al., 1996). This general picture is observed in SGPED40 (Fig. 4C), LCPED20 (Fig. 4E), LCPED40 (Fig. 4F), and NAPED20 (Fig. 4G). However, in the case of possible shallow mixing in Pan de Azúcar (Fig. 4A and B), the homogenization of the nuclide concentration is not resolvable, due to the lack in depth resolution of analysis. For instance, the best Chi-square solution reported for AZPED50 is achieved with a mixing depth of 17.5 cm, whereas the nuclide concentrations do not show a homogenized layer. This depth profile does not reveal a clear picture if the soil layer is mixed or not. The depth profile of SGPED70 (Fig. 4D) shows no clear mixed surface layer. If sample SGPED70_0-5 is the outlier then the mixed surface layer could be 25 cm thick. Assuming sample SGPED70_20-25 is the outlier then the mixed surface layer could be 40 to 70 cm thick. The mobile layer as observed in the field is at 35 cm. The cosmogenic nuclide concentrations in depth profile NAPED40 (Fig. 4H) do not show the expected trend of decreasing concentration with depth. Assuming sample NAPED40_60-65 is the outlier then the mixed surface layer could be interpreted to be

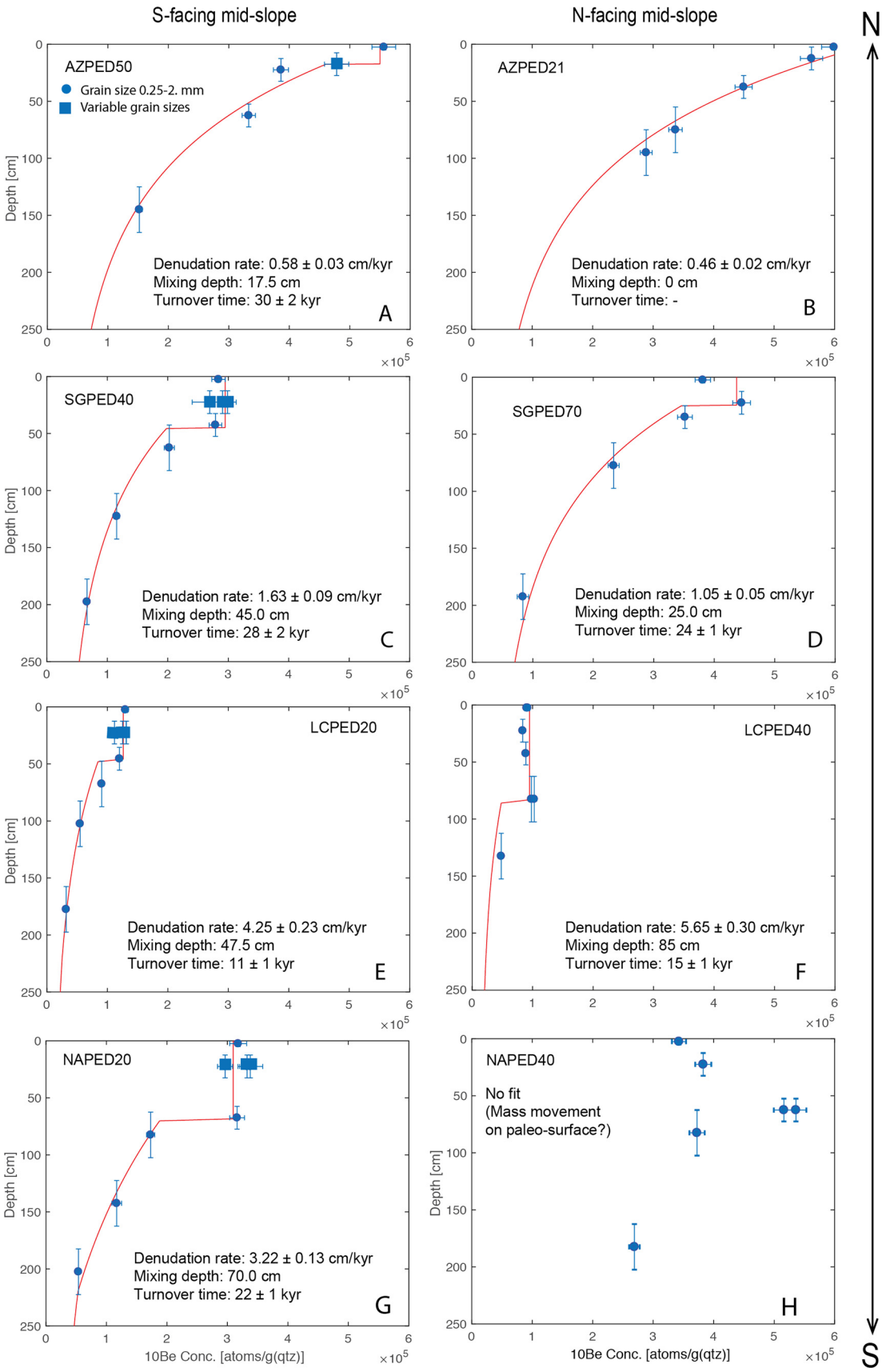

Fig. 4. Diagrams showing depth versus ^{10}Be concentration (blue symbols) for eight mid-slope depth profiles in the four study areas (N to S from top to bottom): Pan de Azúcar (A and B); Santa Gracia (C and D); La Campana (E and F); and Nahuelbuta (G and H). The S-facing profiles are on the left and N-facing profiles on the right. The best solutions for denudation rate and mixing depth based on a Chi-square analysis are reported and plotted (red line). (For interpretation of the colors in the figure(s), the reader is referred to the web version of this article.)

Table 3
Simulations of denudation rates and mixing depths.

Pedon	Production rates			Shielding factor vegetation	Depths		Bulk densities (4 box model)				Denudation rate (cm/kyr)	Mixing depth (cm)	Turnover time (kyr)
	P_{nuc}	P_{muonS}	P_{muonF} (atoms/($g_{(qtz)}$ × yr))		Soil obs. (cm)	Saprolite obs. (cm)	Soil meas. (g/cm^3)	Saprolite meas. (g/cm^3)	Saprolite (g/cm^3)	Rock (g/cm^3)			
AZPED50	3.102	0.011	0.035	1.000	20	220	1.47	1.60	1.60	2.60	0.58 ± 0.03	17.5 ± 0.0/17.5	30 ± 2
AZPED21	3.125	0.011	0.035	1.000	20	220	1.31	1.60	1.60	2.60	0.46 ± 0.02	0.0 ± 12.5/0.0	- ± -
SGPED40	4.231	0.013	0.043	1.000	50	220	1.49	1.60	1.60	2.60	1.63 ± 0.09	45.0 ± 17.5/0.0	28 ± 2
SGPED70	4.259	0.013	0.043	1.000	35	220	1.58	1.60	1.60	2.60	1.05 ± 0.05	25.0 ± 10.0/0.0	24 ± 1
LCPED20	4.454	0.014	0.045	0.977	60	220	1.11	1.48	1.60	2.60	4.25 ± 0.23	47.5 ± 20.0/0.0	11 ± 1
LCPED40	4.477	0.014	0.045	0.977	35	160	1.47	1.55	1.60	2.60	5.65 ± 0.30	85.0 ± 47.5/0.0	15 ± 1
NAPED20	7.148	0.018	0.059	0.927	95	220	0.84	0.92	1.60	2.60	3.22 ± 0.13	70.0 ± 12.5/0.0	22 ± 1
NAPED40	6.930	0.018	0.058	0.927	70	220	0.90	1.21	1.60	2.60			

~100 cm thick. However, sample NAPED40_60-65 could be indicative of a former soil surface overridden by ~50 cm soil material from upslope. If so, the cosmogenic nuclide concentrations of this depth profile cannot be used for model simulations.

Chi-square analysis of measured and modelled cosmogenic nuclide concentrations provides the best solution for a denudation rate and a depth of the mixed layer. All but one depth profile (NAPED40) revealed information about the denudation rate and depth of the mixed mobile layer. Whereas the best solution for AZPED21 indicates no mixed layer, AZPED50 suggests a mixed layer to 17.5 cm. This depth agrees with field observations of a mobile surface layer of 20 cm. In the case of SGPED70 the best solution for the model simulations were achieved with a denudation rate of 1.05 ± 0.05 cm/kyr and a mixed mobile layer of 25 cm (Fig. 4D). This solution indicates that sample SGPED70_0-5 is the outlier. However, if sample SGPED70_20-25 is the outlier and excluded from analysis, then the best solution indicates a denudation rate of 1.08 ± 0.18 cm/kyr and a possible mixing depth to 77.5 cm.

The calculated turnover time, the average time a mineral grain remains in the mobile layer, decreases from Pan de Azúcar (~30 kyr) over Santa Gracia (~26 kyr) to La Campana (~13 kyr). The turnover time in Nahuelbuta (~22 kyr) is higher again. La Campana with the highest denudation rate shows the fastest turnover times despite the thicker mobile layer.

In general, the simulated depths of the mixed layers agree with the mobile layers observed in the field. One exception is LCPED40 where the observed mobile layer is at 35 cm depth, but the modelled mixed layer 85 cm. This difference is attributed to the interpretation of the depth from 35 to 90 cm to be immobile in the field due to the observed compact behavior of this layer. Furthermore, the observed mobile layers in the field generally include A- and B-horizons. However, as simulated cosmogenic nuclide concentrations are based on the assumption of steady-state denudation and complete mixing of the mobile layer, the observation of A- and B-horizons in the field indicate that formation of these horizons have to be fast and ongoing processes as material is eroded from the top.

5.2. Comparison of S- to N-facing slopes in each study area

Differences in denudation rates in S- and N-facing slopes in one area may be the result of investigated different hillslope angles and/or different microclimates on S- and N-facing hillslopes. In general, increasing hillslope angles result in increasing denudation rates (e.g., Binnie et al., 2007). Higher denudation rates in the steeper slope are observed in Pan de Azúcar and Santa Gracia, where these slopes are the S-facing slopes (see Supplementary Fig. S2). In contrast, the steeper N-facing slope in La Campana reports a slower denudation rate than the S-facing slope. Increased denudation rate may not only be attributed to hillslope angle, but may also be affected by hillslope aspect.

Hillslope aspect-driven differences (i.e. N- vs. S-facing) in microclimate may control variations in subsurface rock damage in the regolith (e.g., Hypothesis 3 in Riebe et al., 2017). In N-facing slopes in the Northern hemisphere, solar insolation is lower and ground surface temperatures are cooler than for a S-facing slope which can lead to stronger and deeper frost-cracking (Anderson et al., 2013). This in turn, causes a higher soil production and regolith flux in a N-facing slope than in a S-facing slope, which drives a pronounced asymmetry of hillslope ridges (Anderson et al., 2013). In contrast, the S-facing slopes of our study areas situated in the Southern hemisphere are subjected to lower solar insolation and ground surface temperatures than the N-facing slopes. These lower temperatures result in less evapotranspiration and enable a denser vegetation on the S-facing slopes than the N-facing slopes. However, depending on the vegetation type, increased vegetation cover

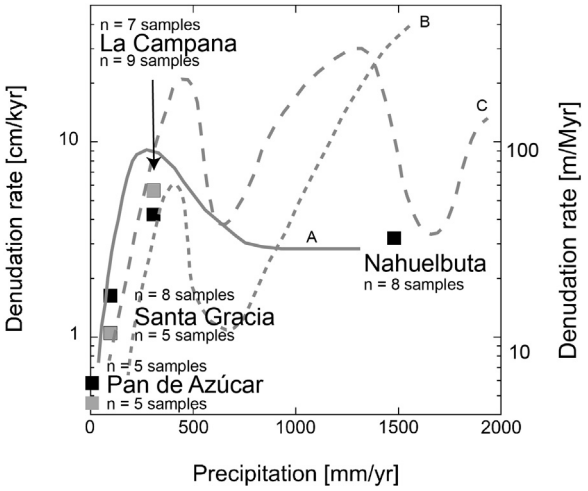

Fig. 5. Denudation rates from cosmogenic depth profiles versus mean annual precipitation. Denudation rates for the S-facing (black squares) and N-facing (gray squares) mid-slope profiles are plotted (except Nahuelbuta N-facing). Denudation rates increase from Pan de Azúcar to La Campana, but are lower in Nahuelbuta than in La Campana. Note that errors are smaller than symbols. For comparison three denudation rate curves as shown in Riebe et al. (2001): A) Curve of Langbein and Schumm (1958) based on ~100 sediment yields of rivers in the USA; B) Curve of Ohmori (1983) based on sediment yields of rivers world-wide; C) Curve of Walling and Webb (1983) based on sediment yields of rivers world-wide.

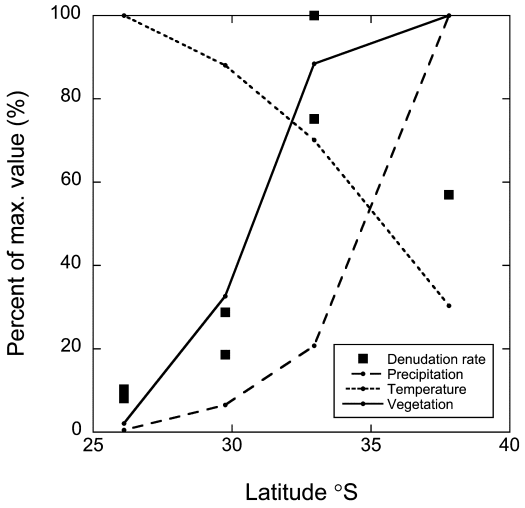

Fig. 6. Percent of maximum value for denudation rate (squares), precipitation (dashed line), temperature (stippled line), and vegetation (bold line) values against latitude. Whereas precipitation and vegetation cover increase from N to S, temperature decreases. In contrast, the denudation rates decrease after a continuous increase to ~35°S.

may either stabilize (e.g., roots) or destabilize (e.g., tree-throw) slopes for denudation. In Pan de Azúcar with a very low MAP and an average vegetation cover of only ~2% a change in vegetation cover and type between hillslopes with different aspect might be minimal. This minimal change might not influence denudation rates (Fig. 5) and depths of mixed layers in the S- and N-facing slopes. Whereas in Santa Gracia the denudation rate is higher on the S-facing slope than the N-facing slope, in La Campana, the denudation rate on the N-facing slope is higher than on the S-facing slope. Changing the amount and type of fauna and flora from S- to N-facing slopes as well as from N to S in latitude may have many different effects on denudation rates. In summary, no clear trend of changes in denudation rates and depths of mobile layers is observed between the S- and N-facing slopes in each of the study areas (Figs. 4 and 5).

5.3. Latitudinal variations in denudation rates from N to S

Hillslope denudation rates are influenced by parameters such as tectonics, climate (including precipitation and temperature), and biota. In order to study the interplay of climate and biota on denudation rates in a climate and vegetation gradient, the tectonic setting should be comparable. Unfortunately, not only are the hillslope scale conditions changing (e.g., hillslope gradient), but also the larger tectonic aspects (e.g., uplift). Whereas hillslope gradients vary from hillslope to hillslope, uplift in the four investigated areas may be different. Whereas uplift rates in Pan de Azúcar and Santa Gracia are comparable and moderate (Melnick, 2016), they are less well-constrained and most likely higher in La Campana and Nahuelbuta. Therefore, when discussing the interplay of climate and biota on hillslope denudation rates in the Chilean Coastal Cordillera, the possible influences of local hillslope gradients and regional uplift rates on denudation rates may not be neglected, although they were minimized as much as possible in our selection of study areas over the latitudinal gradient investigated. Furthermore, we note that within our study areas, there is no evidence for active faulting or mass wasting events. Thus, the hillslopes selected are likely stable and devoid of disturbances due to mass wasting. Thus, any differences in long-term rock uplift rate between the study areas are a) currently poorly know if present, and b) likely regionally driven in nature and not related to active faulting in close proximity to the study areas.

Assuming similarity in the tectonic settings along the Chilean Coastal Cordillera, we try to identify spatial variations in the denudation rates, precipitation, temperature, and vegetation cover (Figs. 5 and 6). However, before these variations are compared, we highlight the difficulties encountered in variables integrating over different time scales. Whereas cosmogenic nuclide-derived denudation rates integrate generally over thousands of years, precipitation, temperature, and vegetation cover are present-day values. Hence, for a comparison to the paleo-climate over the last thousand years this needs to be considered. Paleo-precipitations show similar gradients over the last ~20 kyr as today. Paleo-temperatures did not increase in the S over the last ~20 kyr (see Supplementary Fig. S1), we proceed in comparing denudation rates with precipitation, temperature, and vegetation cover.

Whereas the MAP and the vegetation cover are increasing from N to S in the four study areas, the MAT decreases from N to S (Fig. 6, Table 1). In general, cosmogenic nuclide concentrations and model simulations indicate an increasing depth of the mixed layer from N to S. However, modelled denudation rates only increase from Pan de Azúcar to La Campana. Located south of the La Campana study area, the denudation rate in Nahuelbuta is lower than in La Campana, but higher than in Santa Gracia. Thus, between La Campana and Nahuelbuta a turnover in the trend of denudation rates occurs. In the absence of other evidence, the non-linear change in hillslope denudation rates with increasing latitude that we observe (Figs. 5 and 6, Table 3) is interpreted to result from a changing influence of biota (fauna and flora) on hillslope denudation processes. Increasing vegetation cover from N to S may protect landscapes from enhanced denudation due to increasing precipitation, whereas some types of vegetation cover may reduce hillslope stability (e.g., via tree-throw). For example, whereas the sclerophyllous ecosystem of La Campana has rooting depths of up to 8 m (Giliberto and Estay, 1978), the mixed *Araucaria araucana- Nothofagus dombeyi* forest ecosystem of Nahuelbuta have a much lower rooting depth. Some studies have found that *Nothofagus dombeyi* has fine roots that can be concentrated mainly in the topsoil, with 69% of the total biomass occurring in the top 30 cm of soil and only 1% of root biomass found in 1 m depth (Moreno-Chacón and Lusk, 2004). Also, fauna (e.g., burrowing animals) may increase the

instability of hillslopes. Hence, the complex interaction between climate (MAP and MAT) and biota (fauna and flora) are difficult to disentangle. Each combination of different climate and biota results in a different sensitivity of hillslopes to denudation. For example, variations in denudation rates based on sediment loads in rivers in the USA versus MAP (Curve A in Fig. 5) match well with the hillslope denudation rates from this study. However, more complex relationships between denudation rates based on sediment load of rivers world-wide and MAP are reported (Curve B and C in Fig. 5). The relationship between denudation rates versus MAP do not necessarily display a globally applicable relationship between precipitation rate and denudation, but many different ones that could depend on vegetation differences between the amalgamated data sets.

Furthermore, we have to keep in mind that observed trends between denudation rates, precipitation, and vegetation cover may also be affected by temperature as well as tectonics. The decreasing MAT from N to S may reduce chemical weathering and hence denudation rates from N to S influencing denudation rates in Nahuelbuta differently than in La Campana. Or uplift in La Campana might be more intensive than in Nahuelbuta and be the cause of higher denudation rates in La Campana. In order to better understand how denudation rates are affected by these complex interactions between tectonics, climate, and biota, investigated areas need to be kept as simple as possible.

Taken together, the above discussion on climate, biotic, and tectonic factors influencing hillslopes highlights the complexity in deciphering denudation rates. Theoretical constructs (e.g. coupled geomorphic transport laws) for how biota, climate, and tectonic processes interact on the hillslope scale are largely missing in the literature, and remain a prominent research need. Data sets such as we present here that provide a consistent sampling strategy over a large latitudinal gradient in climate and vegetation provide a first step for evaluating the development of coupled, biotically influenced, transport laws.

6. Conclusions

Here we present eight cosmogenic depth profiles from the mid-slope positions of soil-mantled hillslopes. The *in situ*-produced ^{10}Be concentrations are homogeneous in the surface layer and decrease exponentially with depth below this surface layer. Our analyses of the data indicate that:

i) the surface layer with homogeneous nuclide concentrations generally corresponds to the mobile layer observed in the field. Based on measured ^{10}Be concentrations and model simulations, the mobile layers are, if mixed, well-mixed.

ii) cosmogenic depth profiles from S- and N-facing mid-slope positions report different mixed layer depths as well as denudation rates. Unfortunately, no clear trend is discernible from the available data.

iii) mixed layer depths increase with increasing mean annual precipitation and vegetation cover from N to S. In contrast, denudation rates derived from model simulations of cosmogenic depth profiles not. Denudation rates reach a maximum with a specific mean annual precipitation somewhere between 500–∼1500 mm/yr, mean annual temperature between 7 and 13 °C, and vegetation cover between ∼85–90% (Figs. 5, 6). The increasing vegetation cover may protect the landscape from enhanced denudation by increasing mean annual precipitation, thereby explaining differing results obtained from previous denudation vs. precipitation rates studies. However, as similar climate may be coupled with different biota (e.g. vegetation types), the influence of climate and biota on denudation rates worldwide is difficult to decipher.

Acknowledgements

We thank D. Kost and D. Mühlbayer-Renner for laboratory assistance processing samples. Thoughtful reviews by two anonymous reviewers helped to improve the manuscript. We acknowledge support from the German Science Foundation (DFG) priority research program SPP-1803 “EarthShape: Earth Surface Shaping by Biota” (grant SCHA 1690/3-1 to M. Schaller). We are grateful to the Chilean National Forestry Corporation (CONAF) for providing access to the sample locations and on-site support of our research.

Appendix A. Supplementary material

Supplementary material related to this article can be found online at https://doi.org/10.1016/j.epsl.2018.02.026.

References

Anderson, R.S., Anderson, S.P., Tucker, G.E., 2013. Rock damage and regolith transport by frost: an example of climate modulation of the geomorphology of the critical zone. Earth Surf. Process. Landf. 38, 299–316. https://doi.org/10.1002/esp.3330.

Barnes, J.B., Ehlers, T.A., 2009. End member models for Andean Plateau uplift. Earth-Sci. Rev. 97, 105–132.

Begall, S., Gallardo, M.H., 2000. *Spalacopus cyanus* (Rodentia: Octodontidae): an extremist in tunnel constructing and food storing among subterranean mammals. J. Zool. 251, 53–60. https://doi.org/10.1111/j.1469-7998.2000.tb00592.x.

Bernhard, N., Moskwa, L.-M., Oeser, R., von Blanckenburg, F., Boy, H., Brucker, E., Dippold, M., Ehlers, T.A., Fuentes-Espoz, J.P., Godoy, R., Köster, M., Osses, P., Paulino, L., Schaller, M., Scholten, T., Seguel, O., Spielvogel, S., Spohn, M., Stock, S., Stroncik, N., Uebernickel, K., Wagner, D., Kühn, P., in review. Pedogenic and microbial interrelations to regional climate and local topography: new insights from a climate gradient (arid to humid) along the Coastal Cordillera of Chile. Catena.

Binnie, S.A., Phillips, W.M., Summerfield, M.A., Fifield, L.K., 2007. Tectonic uplift, threshold hillslopes, and denudation rates in a developing mountain range. Geology 35, 743–746. https://doi.org/10.1130/G23641A.1.

Borchers, B., Marrero, S., Balco, G., Caffee, M., Goehring, B., Lifton, N., Nishiizumi, K., Phillips, F., Schaefer, J., Stone, J., 2016. Geological calibration of spallation production rates in the CRONUS-Earth project. Quat. Geochronol. 31, 188–198. https://doi.org/10.1016/j.quageo.2015.01.009.

Braucher, R., Merchel, S., Borgomano, J., Bourlès, D.L., 2011. Production of cosmogenic radionuclides at great depth: a multi element approach. Earth Planet. Sci. Lett. 309, 1–9. https://doi.org/10.1016/j.epsl.2011.06.036.

Brown, E.T., Stallard, R.F., Larsen, M.C., Raisbeck, G.M., Yiou, F., 1995. Denudation rates determined from the accumulation of in situ-produced ^{10}Be in the Luquillo Experimental Forest, Puerto Rico. Earth Planet. Sci. Lett. 129, 193–202.

Broxton, P.D., Zeng, X., Scheftic, W., Troch, P.A., 2014. A MODIS-based global 1-km maximum green vegetation fraction dataset. J. Appl. Meteorol. Climatol. 53, 1996–2004.

Chmeleff, J., von Blanckenburg, F., Kossert, K., Jakob, D., 2010. Determination of the ^{10}Be half-life by multicollector ICP-MS and liquid scintillation counting. Nucl. Instrum. Methods Phys. Res., Sect. B, Beam Interact. Mater. Atoms 268, 192–199. https://doi.org/10.1016/j.nimb.2009.09.012.

Corenblit, D., Baas, A.C.W., Bornette, G., Darrozes, J., Delmotte, S., Francis, R.A., Gurnell, A.M., Julien, F., Naiman, R.J., Steiger, J., 2011. Feedbacks between geomorphology and biota controlling Earth surface processes and landforms: a review of foundation concepts and current understandings. Earth-Sci. Rev. 106, 307–331. https://doi.org/10.1016/j.earscirev.2011.03.002.

Cui, L.-F., Liu, C.-Q., Xu, S., Zhao, Z.-Q., Liu, T.-Z., Liu, W.-J., Zhang, Z.-J., 2016. Subtropical denudation rates of granitic regolith along a hill ridge in Longnan, SE China derived from cosmogenic nuclide depth-profiles. J. Asian Earth Sci. 117, 146–152. https://doi.org/10.1016/j.jseaes.2015.12.006.

Ebensperger, L.A., Bozinovic, F., 2000. Communal burrowing in the hystricognath rodent, *Octodon degus*: a benefit of sociality? Behav. Ecol. Sociobiol. 47, 365–369.

Ebensperger, L.A., Chesh, A.S., Castro, R.A., Tolhuysen, L.O., Quirici, V., Burger, J.R., Sobrero, R., Hayes, L.D., 2011. Burrow limitations and group living in the communally rearing rodent, *Octodon degus*. J. Mammal. 92 (1), 21–30. https://doi.org/10.1644/09-MAMM-S-383.1.

Giliberto, J., Estay, H., 1978. Seasonal water stress in some Chilean matorral shrubs. Botanical Gazette 139, 236–240.

Granger, D.E., Riebe, C.S., 2014. Cosmogenic nuclides in weathering and erosion. In: Treatise on Geochemistry. Elsevier, pp. 401–436.

Granger, D.E., Kirchner, J.W., Finkel, R., 1996. Spatially averaged long-term erosion measured from in situ-produced cosmogenic nuclides in alluvial sediment. J. Geol. 104, 249–257.

Hauck, L., Moreira-Muñoz, A., Nezadal, W., 2016. The exotic ruderal flora of La Campana National Park, Valparaíso Region, central Chile. Gayana Botanica 73, 206–219.

Heimsath, A.M., Dietrich, W.E., Nishiizumi, K., Finkel, R.C., 1997. The soil production function and landscape equilibrium. Nature 388, 358–361.

Hidy, A.J., Gosse, J.C., Pederson, J.L., Mattern, J.P., Finkel, R.C., 2010. A geologically constrained Monte Carlo approach to modeling exposure ages from profiles of cosmogenic nuclides: an example from Lees Ferry, Arizona. Geochem. Geophys. Geosyst. 11. https://doi.org/10.1029/2010GC003084.

Jara-Muñoz, J., Melnick, D., Brill, D., Strecker, M.R., 2015. Segmentation of the 2010 Maule Chile earthquake rupture from a joint analysis of uplifted marine terraces and seismic-cycle deformation patterns. Quat. Sci. Rev. 113, 171–192. https://doi.org/10.1016/j.quascirev.2015.01.005.

Juez-Larré, J., Kukowski, N., Dunai, T.J., Hartley, A.J., Andriessen, P.A.M., 2010. Thermal and exhumation history of the Coastal Cordillera arc of northern Chile revealed by thermochronological dating. Tectonophysics 495, 48–66. https://doi.org/10.1016/j.tecto.2010.06.018.

Karger, D.N., Conrad, O., Böhner, J., Kawohl, T., Kraft, H., Soria-Auza, R.W., Zimmermann, N.E., Linder, H.P., Kessler, M., 2017. Climatologies at high resolution for the Earth's land surface areas. Sci. Data 4. https://doi.org/10.1038/sdata.2017.122.

Korschinek, G., Bergmaier, A., Faestermann, T., Gerstmann, U.C., Knie, K., Rugel, G., Wallner, A., Dillmann, I., Dollinger, G., von Gostomski, C.L., Kossert, K., Maiti, M., Poutivtsev, M., Remmert, A., 2010. A new value for the half-life of ^{10}Be by heavy-ion elastic recoil detection and liquid scintillation counting. Nucl. Instrum. Methods Phys. Res., Sect. B, Beam Interact. Mater. Atoms 268, 187–191. https://doi.org/10.1016/j.nimb.2009.09.020.

Langbein, W.B., Schumm, S.A., 1958. Yield of sediment in relation to mean annual precipitation. Eos Trans. AGU 39, 1076–1084. https://doi.org/10.1029/TR039i006p01076.

Lifton, N.A., Sato, T., Dunai, T.J., 2014. Scaling in situ cosmogenic nuclide production rates using analytical approximations to atmospheric cosmic-ray fluxes. Earth Planet. Sci. Lett. 386, 149–160. https://doi.org/10.1016/j.epsl.2013.10.052.

Luebert, F., Pliscoff, P., 2006. Sinopsis bioclimática y vegetacional de Chile. Editorial Universitaria. ISBN 9561118327, 9789561118324, 316 p.

Marrero, S.M., Phillips, F.M., Borchers, B., Lifton, N., Aumer, R., Balco, G., 2016. Cosmogenic nuclide systematics and the CRONUScalc program. Quat. Geochronol. 31, 160–187.

Melnick, D., 2016. Rise of the central Andean coast by earthquakes straddling the Moho. Nat. Geosci. 9, 401–407. https://doi.org/10.1038/ngeo2683.

Moreno-Chacón, M., Lusk, C.H., 2004. Vertical distribution of fine root biomass of emergent *Nothofagus dombeyi* and its canopy associates in a Chilean temperate rainforest. For. Ecol. Manag. 199, 177–181.

Mutz, S.G., Ehlers, T.A., Werner, M., Lhmann, G., Stepanek, C., Li, J., 2017. Where is Late Cencozoic climate change most likely to impact denudation? Earth Surf. Dyn. https://doi.org/10.5194/esurf-2017-47.

Ohmori, H., 1983. Erosion rates and their relation to vegetation from the view-point of worldwide distribution. Bull. Depart. Geogr. Univ. Tokyo 15, 77–91.

Owen, J.J., Amundson, R., Dietrich, W.E., Nishiizumi, K., Sutter, B., Chong, G., 2011. The sensitivity of hillslope bedrock erosion to precipitation. Earth Surf. Process. Landf. 36, 117–135. https://doi.org/10.1002/esp.2083.

Plug, L.J., Gosse, J.C., McIntosh, J.J., Bigley, R., 2007. Attenuation of cosmic ray flux in temperate forest. J. Geophys. Res. 112, F02022. https://doi.org/10.1029/2006JF000668.

Riebe, C.S., Granger, D., 2013. Quantifying deep and near-surface chemical erosion on cosmogenic nuclides in soils, saprolite, and sediment. Earth Surf. Process. Landf. 38, 523–533.

Riebe, C.S., Hahm, W.J., Brantley, S.L., 2017. Controls on deep critical zone architecture: a historical review and four testable hypotheses: four Testable Hypotheses about the Deep Critical Zone. Earth Surf. Process. Landf. 42, 128–156. https://doi.org/10.1002/esp.4052.

Riebe, C.S., Kirchner, J.W., Granger, D.E., Finkel, R.C., 2001. Minimal climatic control on erosion rates in the Sierra Nevada, California. Geology 29, 447–450.

Rundel, P.W., Weisser, P.J., 1975. La Campana, a new National Park in central Chile. Biol. Conserv. 8, 35–46.

Schaller, M., Ehlers, T.A., Blum, J.D., Kallenberg, M.A., 2009. Quantifying glacial moraine age, denudation, and soil mixing with cosmogenic nuclide depth profiles. J. Geophys. Res., Earth Surf. 114, F01012. https://doi.org/10.1029/2007JF00921.

Teta, P., Pardiñas, U.F.J., D'Elía, G., 2015a. Genus *Chelemys* Thomas, 1903. In: Patton, J.L., Pardiñas, F.J., D'Elía, G. (Eds.), Mammals of South America. Volume 2: Rodents. The University of Chicago Press, p. 127.

Teta, P., Pardiñas, U.F.J., D'Elía, G., 2015b. Genus *Geoxus* Thomas, 1919. In: Patton, J.L., Pardiñas, F.J., D'Elía, G. (Eds.), Mammals of South America. Volume 2: Rodents. The University of Chicago Press, p. 132.

Thompson, M.V., Palma, B., Knowles, J.T., Holbrook, M., 2003. Multi-annual climate in Parque Nacional Pan de Azúcar, Atacama Desert, Chile. Rev. Chil. Hist. Nat. 76, 235–254.

Vázquez, M., Ramírez, S., Morata, D., Reich, M., Braun, J.-J., Carretier, S., 2016. Regolith production and chemical weathering of granitic rocks in central Chile. Chem. Geol. 446, 87–98. https://doi.org/10.1016/j.chemgeo.2016.09.023.

Walling, D.E., Webb, B.W., 1983. Patterns of sediment yield. In: Gregory, K.J. (Ed.), Background to Paleohydrology. John Wiley and Sons, Chichester, U.K., pp. 69–100.

Zamorano-Elgueta, C., Cayuela, L., González-Espinosa, M., Lara, L., Parra-Vázquez, M.R., 2012. Impacts of cattle on the South American temperate forests: challenges for the conservation of the endangered monkey puzzle tree (*Araucaria araucana*) in Chile. Biol. Conserv. 152, 110–118.